Evaluation of a ferroelectric tunnel junction by ultraviolet–visible absorption using a removable liquid electrode

2016 Nanotechnology 27 215704

(http://iopscience.iop.org/0957-4484/27/21/215704)

IOP Publishing Nanotechnology
Nanotechnology 27 (2016) 215704 (6pp) doi:10.1088/0957-4484/27/21/215704

Evaluation of a ferroelectric tunnel junction by ultraviolet–visible absorption using a removable liquid electrode

Hong-Sub Lee[1], Kyung-Mun Kang[1], Geun Young Yeom[2] and Hyung-Ho Park[1]

[1] Department of Materials Science and Engineering, Yonsei University, Seodaemun-Ku, Seoul 120-749, Korea
[2] Department of Advanced Materials Science and Engineering and SKKU Advanced Institute of Nanotechnology, Sungkyunkwan University, Suwon, Kyunggi-do 440-746, Korea

E-mail: hhpark@yonsei.ac.kr

Received 21 January 2016, revised 2 March 2016
Accepted for publication 24 March 2016
Published 18 April 2016

Abstract

Ferroelectric memristors offer a significant alternative to their redox-based analogs in resistive random access memory because a ferroelectric tunnel junction (FTJ) exhibits a memristive effect that induces resistive switching (RS) regardless of the operating current level. This RS results from a change in the ferroelectric polarization direction, allowing the FTJ to overcome the restriction encountered in redox-based memristors. Herein, the memristive effect of an FTJ was investigated by ultraviolet–visible (UV–Vis) absorption spectroscopy using a removable mercury (Hg) top electrode (TE), $BaTiO_3$ (BTO) ferroelectric tunnel layer, $La_{0.7}Sr_{0.3}MnO_3$ (LSMO) semiconductor bottom electrode, and wide-bandgap quartz (100) single-crystal substrate to determine the low-resistance state (LRS) and high-resistance state (HRS) of the FTJ. A BTO (110)/LSMO (110) polycrystal memristor involving a Hg TE showed a small memristive effect (switching ratio). This effect decreased with increasing read voltage because of a small potential barrier height. The LRS and HRS of the FTJ showed quasi-similar UV–Vis absorption spectra, consistent with the small energy difference between the valence-band maximum of BTO and Fermi level of LSMO near the interface between the LRS and HRS. This energy difference stemmed from the ferroelectric polarization and charge-screening effect of LSMO based on an electrostatic model of the FTJ.

Keywords: ferroelectric tunnel junction, memristor, ultraviolet–visible absorption, electrostatic model, resistive random access memory

(Some figures may appear in colour only in the online journal)

1. Introduction

The development of next-generation nonvolatile memory (NVM) that exhibits low power consumption and high density is required to overcome the restrictions of current memory devices such as dynamic random access memory (RAM) and NAND flash memory. Existing NVM candidates such as ferroelectric RAM, resistive RAM, magnetic RAM, and phase-change RAM rely on state variations caused by the resistance change of materials, as described by their names, instead of a current charge trap method [1–8]. Therefore, materials play a key role in NVM realization. Specifically, because of the simple metal–insulator–metal (MIM) configuration of resistive RAM devices using redox-based memristors, they have attracted considerable attention in the generation of cross-point array structures presenting the highest-density integration [9–12]. However, the high operating current level and low reliability of these memristors have hindered the development of resistive RAM. Redox-based memristors depend on a resistive switching (RS)

mechanism, which restricts the reduction of their operating current and resistance dispersion [13, 14]. They require sufficient voltage and high current to switch their resistance state by electrochemical migration and/or redox. Ferroelectric memristors have emerged as promising alternatives to these resistive RAM devices because the memristive effect of a ferroelectric tunnel junction (FTJ) induces RS through a change in the ferroelectric polarization direction regardless of the operating current level [15–17]. Therefore, in this study, this memristive effect is applied to resistive RAM to minimize the operating current level and resistance dispersion. This effect results from a change in the average potential barrier height with respect to the remnant polarization direction of an ultrathin ferroelectric layer, which requires metal and semiconductor asymmetric top and bottom electrodes [18]. In the metal electrode/ferroelectric tunnel layer (FTL)/semiconductor electrode structure, variations in the Thomas–Fermi screening length of the asymmetric electrodes alter the average potential barrier height for different tunneling currents [19]. Therefore, the use of different top and bottom electrodes is critical for RS. Changes at the FTL/semiconductor electrode interface were investigated using a drop of mercury (Hg) as the top electrode (TE), $BaTiO_3$ (BTO) as FTL, $La_{0.7}Sr_{0.3}MnO_3$ (LSMO) as the semiconductor bottom electrode (BE), and single-crystal quartz (100) as the substrate. The association of the Hg drop TE with the quartz substrate, which presented a wide bandgap (>7.8 eV), facilitated ultraviolet–visible (UV–Vis) absorption measurements after resistance state switching. The final states of the FTJ, known as the high-resistance state (HRS) and low-resistance state (LRS), were evaluated by UV–Vis absorption using a removable liquid electrode.

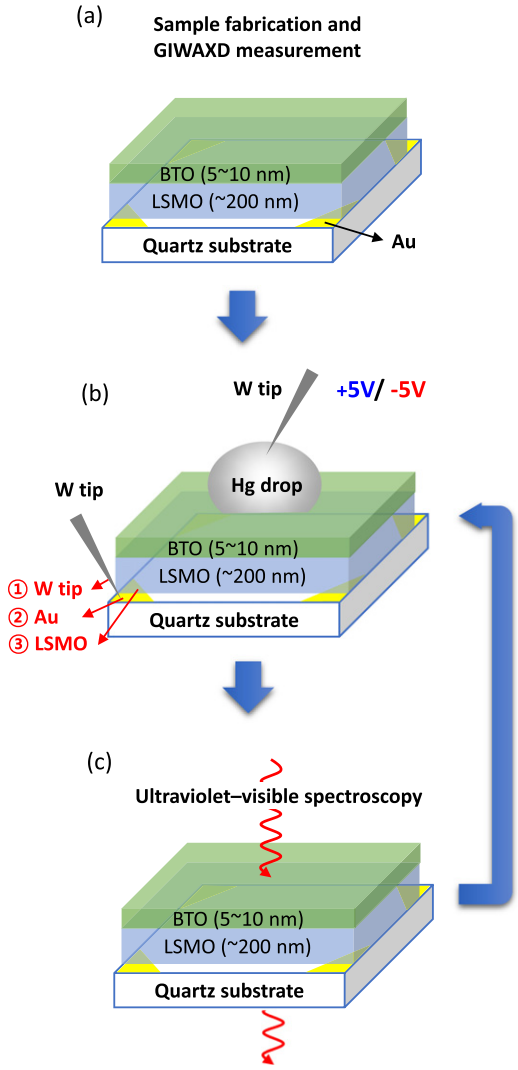

Figure 1. Schematic of experimental procedures. (a) Fabrication of BTO/LSMO/quartz and GI-WAXD measurements; (b) LRS/ HRS switching using a Hg drop; (c) UV–Vis absorption measurement of each LRS and HRS.

2. Experimental details

Au contact electrode ② (work function: ~5.1 eV) was formed at the corner of the quartz (100) substrate (20 mm × 20 mm) to achieve an ohmic contact between tungsten tip ① (work function: ~4.4 eV) and LSMO p-type semiconductor (and/or half metallic) BE ③ (work function: ~4.8 eV) (figure 1(b)). Subsequently, FTL (thickness: 5–10 nm) and BE (thickness: ~200 nm) were deposited on the substrate by *in situ* radio-frequency magnetron sputtering. BTO and LSMO sputter targets were prepared by a standard solid-state reaction method using Ba_2O_3, Ti_2O_3, La_2O_3, $SrCO_3$, and Mn_2O_3 powders as starting materials. During the deposition, the working pressure, substrate temperature, and Ar/O_2 gas flow ratio were maintained at 20 mTorr, 550 °C, and 4:1, respectively. Phase formation and crystallinity were monitored by grazing-incidence wide-angle x-ray diffraction (GI-WAXD) at the Pohang Accelerator Laboratory using monochromatic radiation ($\lambda = 0.620831$ Å). The x-ray irradiation time ranged between 2 and 120 s depending on the detector saturation level. Diffraction angles were calibrated using precalibrated sucrose (monoclinic, $P2_1$, $a = 10.8631$ Å, $b = 8.7044$ Å, $c = 7.7624$ Å, $\beta = 102.938°$). The sample-detector distance was set to 223.3 mm. The RS behavior of the Hg/BTO (110)/LSMO (110) structure was determined by a two-probe method using a Keithley 2635A sourcemeter. Current–voltage (*I–V*) characteristics of the films were determined using a removable Hg drop TE. All measurements were performed at room temperature. Absorption rates of the LRS and HRS were obtained using a UV–Vis spectrophotometer (V-570, JASCO).

3. Results and discussion

Figure 1 shows a schematic of sample formation, *I–V* measurement using the removable Hg TE, and UV–Vis absorption measurement. The crystal structure of the fabricated BTO/LSMO/quartz sample (figure 1(a)) was determined by GI-WAXD. The resulting two-dimensional image revealed that BTO and LSMO preferably adopted an in-plane (110) orientation (blue box, figure 2(a)) [20]. In contrast, Au showed a ring pattern corresponding to a randomly oriented

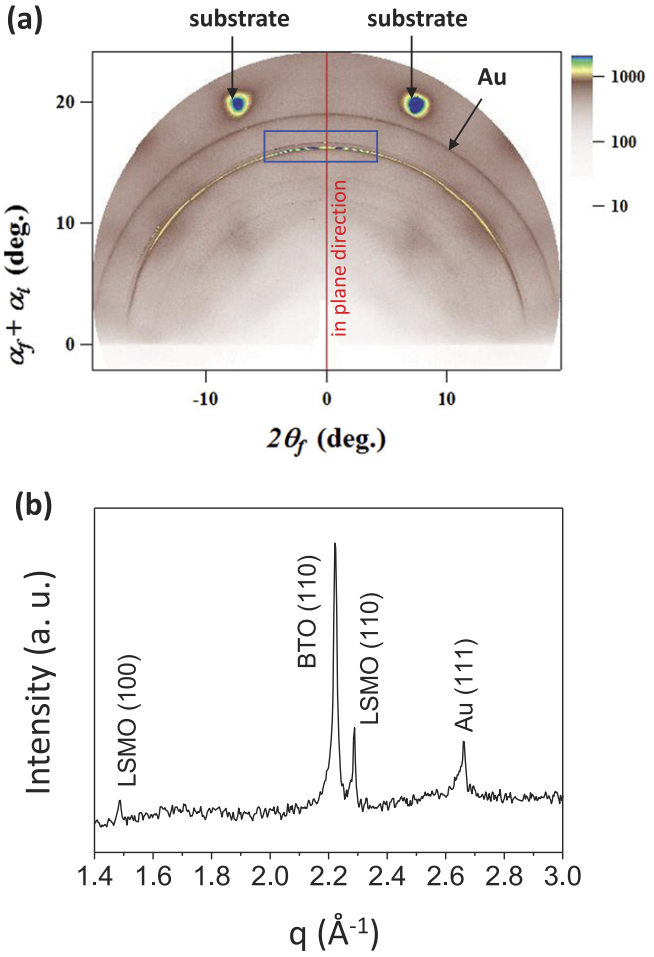

Figure 2. (a) Two-dimensional and (b) one-dimensional GI-WAXD (vertical cut) data of BTO/LSMO/Au (contact electrode)/ quartz (100).

polycrystal. A one-dimensional pattern was derived from the GI-WAXD data (red line, figure 2(a)), which showed in-plane LSMO (100), BTO (110), LSMO (110), and Au (111) diffraction peaks (figure 2(b)). The uppermost ultrathin BTO layer displayed a large diffraction peak at a grazing-incidence angle of 0.05°. D-spacing values calculated from diffraction peak positions are 4.422, 2.826, 2.748, and 2.358 Å for LSMO (100), BTO (110), LSMO (110), and Au (111), respectively. Moreover, these data suggest that a BTO film adopted a tetragonal phase (JCPDS: 05-0626).

The FTL was investigated by using piezoresponse force microscopy with BTO/ LSMO/ quartz (100) sample. The local out-of-plane piezoresponses such as phase and amplitude signals of bare surface of BTO/ LSMO/ quartz (100) were given in figures 3(a) and (b), respectively. BTO/ LSMO/ quartz (100) structure shows small amplitude while hysteretic behavior with 180° phase difference was observed due to a preferred orientation of BTO (110) plane. Memristive characteristics were determined using DC bias sweep and an operating cycle as shown in figures 3(c) and (d) by *I–V* measurement of metal TE (Hg liquid drop)/FTL/semiconductor BE structure. After we put Hg liquid drop on BTO/ LSMO/ quartz (100) surface, tungsten tips contacted the removable Hg drop TE and Au contact electrode as shown in figure 1(b). The figure 3(c) shows memristive characteristic during repeated *I–V* measurements. The memristive characteristic (memory window) was small while BTO/ LSMO/ quartz (100) clearly shows hysteretic *I–V* curve caused by small ferroelectric amplitude and defects of polycrystal FTL. For an endurance test, operating cycle was set as figure 3(d) where the current level (resistance state) was determined 10 times at read voltage (V_{read}) values of +0.1, +0.2, +0.5, and +1 V after a writing operation using an amplitude of ±5 V and pulse width of 500 μs. A single cycle, which comprised one writing and 10 reading operations (figure 3(a)), was repeated 10 times (20th writing and 200th reading, figure 3(b)). The switching ratio R_{HRS}/R_{LRS} (sensing margin) was very small and amounted to 1.97, 1.16, 1.03, and 1.01 for V_{read} values of +0.1, +0.2, +0.5, +1 V, respectively. The V_{read}-dependent decrease in the switching ratio might have resulted from the low potential barrier height of a BTO tunneling layer by defects and/or polycrystal FTL. In general, MIM structures follow a carrier transport mechanism involving a direct tunneling (J_{DT}) → Fowler–Nordheim tunneling (J_{FNT}) → thermionic emission (J_{TI}) sequence with an increasing voltage [16]. Therefore, a relatively lower potential barrier height of the BTO tunneling layer induces J_{TI} at a relatively lower voltage. In fact, the resulting memristive effect can be reduced to a greater extent in the J_{TI} regime compared with J_{DT} and J_{FNT} regimes [15–17]. In general, an increase in defects inside a ferroelectric insulating layer increases the Fermi level of the BTO layer, lowering the potential barrier height [17].

Figure 4(a) shows a Tauc plot [21] of UV–Vis absorption spectra as a function of photon energy for the LRS and HRS acquired in the absence of the removable Hg TE (figure 1(c)). An expanded region of photon energy (inset) revealed a small difference in UV absorption between the LRS and HRS at 1.38 eV of photon energy. Specifically, compared to the HRS, the LRS exhibited a 0.064% reduction in the absorption rate at 1.38 eV as its absorption shifted by approximately 0.055 eV to a higher energy level for the same absorption rate. The extrapolation to zero of the linear portion of the extended curve (up to a photon energy of 6 eV) provides the optical bandgap of the BTO layer at each switching state [22]. In general, the UV absorption rate and/ or gradient depend on the film thickness and/or band shape. The UV–Vis absorption spectra of the LRS and HRS were obtained using the same sample (figure 1), indicating that the thickness was constant. Therefore, absorption rate differences may originate from changes in the band shape and/or band bending. Calculated optical bandgaps for the LRS and HRS amounted to 3.026 and 3.081 eV, respectively, and these values may be attributed to the optical bandgap of the BTO layer. Schematic band diagrams using an electrostatic model of the FTJ are proposed in figure 4(b) for the LRS and HRS to interpret the small difference in optical bandgaps. For a UV photon passing through the quartz substrate, LSMO, and BTO, the small absorption difference is expected to stem from BTO/LSMO interfacial changes because a BTO FTL itself should display the same absorption in the LRS and

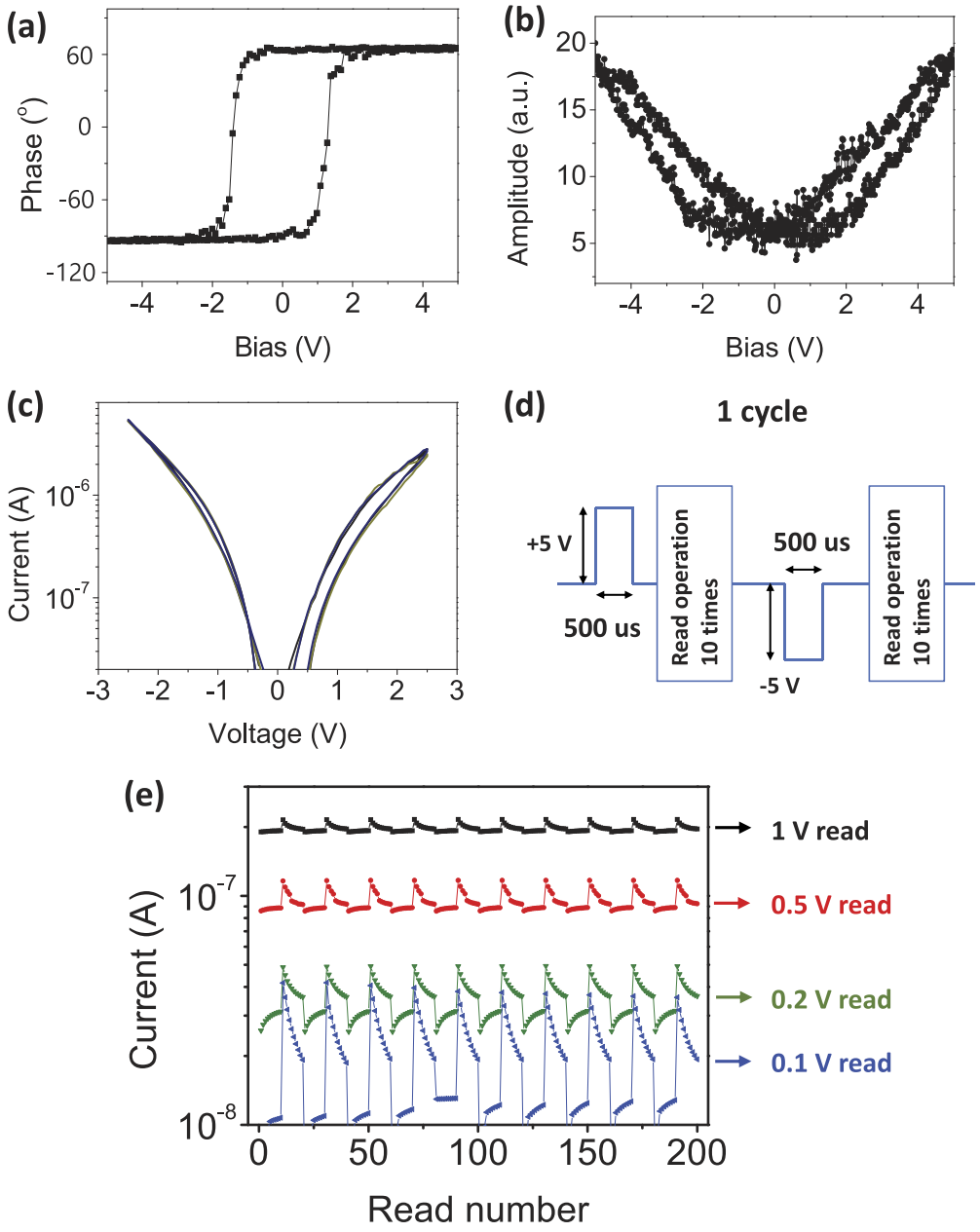

Figure 3. Hysteretic behavior of BTO/ LSMO/ quartz (100): (a) amplitude and (b) phase signals. (c) *I–V* characteristic of Hg/BTO/LSMO/ Au (contact electrode) by DC bias sweep. (d) Memristive effect measurement program and (e) memristive characteristics of Hg/BTO/ LSMO/Au (contact electrode) at various read voltages.

HRS regardless of the polarization direction. However, the charge-carrier density changed according to ferroelectric polarization direction and screened the ferroelectric polarization in the presence of a potential barrier near the interface (charge-screening effect, figure 4(b)) [23, 24]. When LSMO is considered as a p-type semiconductor, an increase in the electron concentration and thus a decrease in the hole concentration near the interface may occur to screen the downward polarization of the ferroelectric layer. In addition, the charge-screening length 'δ' depends on the carrier concentration in the LSMO semiconductor. Therefore, it remained the same for the LRS and HRS regardless of the ferroelectric polarization direction while the potential barrier height varied. For the LRS, the energy difference between the valence-band maximum (VBM) of the BTO layer and the Fermi level of the LSMO p-type semiconductor layer increased due to the downward polarization. Concurrently, the potential barrier height corresponding to the energy distance between the electron affinity of the BTO layer and the Fermi level of LSMO decreased. As suggested by the ferroelectric polarization direction, the HRS showed the opposite behavior. Therefore, the relatively higher absorption rate of the HRS originated from the relatively smaller energy distance between the VBM of the BTO layer and the Fermi level of LSMO. As a result, changes occurring near the interface between the LRS and HRS slightly alter UV–Vis absorption spectra. Memristive effect (RS) and UV absorption differences detected in this study were small. However,

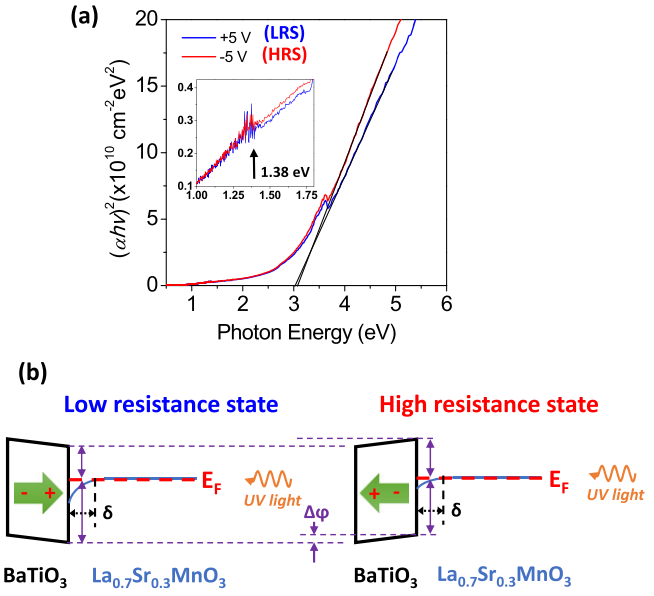

Figure 4. (a) A Tauc plot of UV–Vis absorption spectra of LRS and HRS in BTO/LSMO/quartz (100) from 0.5 to 6 eV (inset: expanded spectra for photon energies ranging from 1.0 to 1.8 eV) and (b) schematic band diagrams of LRS and HRS based on electrostatic model of ferroelectric tunnel junction.

the spectral phenomenon observed along the ferroelectric polarization direction in an FTJ sample, such as BTO/LSMO, provides useful information of the memristive effect of an FTJ in terms of band bending and potential barrier changes near interfaces.

4. Conclusion

The memristive characteristics of a ferroelectric tunnel device using a Hg drop TE and wide-bandgap quartz substrate were investigated by UV–Vis absorption spectroscopy. The BTO (110)/LSMO (110) polycrystalline memristor in the presence of the Hg TE showed a small memristive effect with a switching ratio of 1.97 at +0.1 V_{read}. This memristive effect decreased with increasing read voltage because of a low potential barrier height. Removable Hg drop TE and quartz substrate with a wide bandgap (>7.8 eV) facilitated UV–Vis absorption measurements after RS. A small absorption difference was observed between the LRS and HRS as a result of changes in the ferroelectric polarization direction near their interface. In particular, the BTO/LSMO interface exhibited a higher absorption rate for the HRS compared with the LRS. A combination of UV–Vis absorption data with an electrostatic model of the FTJ suggested that the spectral difference stemmed from the smaller energy difference between the VBM of the BTO layer and the Fermi level of LSMO near the interface induced by the ferroelectric polarization and charge-screening effect of the LSMO layer.

Acknowledgments

This work was supported by the Industrial Strategic Technology Development Program (10041926, Development of high density plasma technologies for thin film deposition of nanoscale semiconductor and flexible display processing) funded by the Ministry of Knowledge Economy (MKE, Korea). This work was supported by the National Research Foundation of Korea (NRF) grant funded by the Korea government (MSIP) (No. 2015R1A2A1A15054541). The experiments at the PLS were supported in part by MSIP and POSTECH.

References

[1] Garcia V and Bibes M 2014 Ferroelectric tunnel junctions for information storage and processing *Nat. Commun.* **5** 4289
[2] Ramesh R and Spaldin N A 2007 Multiferroics: progress and prospects in thin films *Nat. Mater.* **6** 21
[3] Wuttig M 2005 Phase-change materials: towards a universal memory? *Nat. Mater.* **4** 265
[4] Chappert C, Fert A and Van Dau F N 2007 The emergence of spin electronics in data storage *Nat. Mater.* **6** 813
[5] Lee H S, Choi S G, Park H H and Rozenberg M J 2013 A new route to the Mott–Hubbard metal–insulator transition: strong correlations effects in $Pr_{0.7}Ca_{0.3}MnO_3$ *Sci. Rep.* **3** 1704
[6] Szot K, Speier W, Bihlmayer G and Waser R 2006 Switching the electrical resistance of individual dislocations in single-crystalline $SrTiO_3$ *Nat. Mater.* **5** 312
[7] Lee H-S, Park C-S and Park H-H 2014 Effect of La^{3+} substitution with Gd^{3+} on the resistive switching properties of $La_{0.7}Sr_{0.3}MnO_3$ thin films *Appl. Phys. Lett.* **104** 191604
[8] Chabi D, Wang Z, Bennett C and Klein J-O 2015 A physics-based compact model of ferroelectric tunnel junction for memory and logic design *IEEE Trans. Nanotechnol.* **14** 954
[9] Linn E, Rosezin R, Kügeler C and Waser R 2010 Complementary resistive switches for passive nanocrossbar memories *Nat. Mater.* **9** 403
[10] Yang J J, Pickett M D, Li X, Ohlberg D A A, Stewart D R and Williams R S 2008 A fast, high-endurance and scalable non-volatile memory device made from asymmetric Ta_2O_{5-x}/TaO_{2-x} bilayer structures *Nat. Nanotechnol.* **3** 429
[11] Lee M-J *et al* 2011 A fast, high-endurance and scalable non-volatile memory device made from asymmetric Ta_2O_{5-x}/TaO_{2-x} bilayer structures *Nat. Mater.* **10** 625
[12] Lee H-S, Park H-H and Rozenberg M J 2015 Manganite-based memristive heterojunction with tunable nonlinear *I–V* characteristics *Nanoscale* **7** 6444
[13] Waser R, Dittmann R, Staikov G and Szot K 2009 Redox-based resistive switching memories-nanoionic mechanisms prospects, and challenges *Adv. Mater.* **21** 2632
[14] Lee H-S, Yeom G Y and Park H-H 2015 Investigation into the influence of interfacial changes on the resistive switching of $Pr_{0.7}Ca_{0.3}MnO_3$ *J. Phys. D: Appl. Phys.* **48** 465309
[15] Wang Z, Zhao W, Kang W, Zhang Y, Klein J-O, Ravelosona D and Chappert C 2014 Compact modelling of ferroelectric tunnel memristor and its use for neuromorphic simulation *Appl. Phys. Lett.* **104** 053505
[16] Pantel D and Alexe M 2010 Electroresistance effects in ferroelectric tunnel barriers *Phys. Rev.* B **82** 134105
[17] Lee H-S, Han W, Chung H-Y, Rozenberg M, Kim K, Lee Z, Yeom G Y and Park H-H 2015 Ferroelectric tunnel junction for dense cross-point arrays *ACS Appl. Mater. Interfaces* **7** 22348

[18] Gruverman A 2009 Tunneling electroresistance effect in ferroelectric tunnel junctions at the nanoscale *Nano Lett.* **9** 3539

[19] Chanthbouala A *et al* 2011 A solid-state memories based on ferroelectric tunnel junctions *Nat. Nanotechnol.* **7** 101

[20] Yang S Y, Kuang W L, Liou Y, Tse W S, Lee S F and Yao Y D 2003 Growth and characterization of $La_{0.7}Sr_{0.3}MnO_3$ films on various substrates *J. Magn. Magn. Mater.* **268** 326

[21] Tauc J 1970 Absorption edge and internal electric fields in amorphous semiconductors *Mater Res. Bull.* **5** 721

[22] Choi Y-J and Park H-H 2014 A simple approach to the fabrication of fluorinedoped zinc oxide thin films by atomic layer deposition at low temperatures and an investigation into the growth mode *J. Mater. Chem.* C **2** 98

[23] Chanthbouala A *et al* 2012 A ferroelectric memristor *Nat. Mater.* **11** 860

[24] Soni R, Petraru A, Meuffels P, Vavra O, Ziegler M, Kim S K, Jeong D S, Pertsev N A and Kohlstedt H 2014 Giant electrode effect on tunneling electroresistance in ferroelectric tunnel junctions *Nat. Commun.* **5** 5414